Tank Test of an Active Power Rectification in Wave-to-Wire Energy Conversion

Chien-An Chen, Xiaofan Li, Dillon Martin, and Lei Zuo

Abstract—**Maximum power control algorithms in wave energy converter (WEC) are mainly based on the fluid-structure dynamics with impedance matching from power take-off (PTO) damping or model predictive control through the buoy dynamics. However, the conventional buoy characteristics study cannot satisfy estimation of maximum output power in a practical wave-to-wire (W2W) system due to significant losses on mechanical and electrical components from PTO to power converter in comparison with the losses on the buoy. To analysis the non-ideal effects from mechanical transmission and energy conversion characteristics of WEC with a power converter output, a W2W simulation and tank testing is performed. The 1:20 scale WEC system with 1.17m buoy diameter includes a single body heaving buoy, mechanical-motion-rectifier based power-take-off, and power converter that store its output energy to a battery load. From the tank testing results, a circuit model is built and is used to estimate the system performance. The non-ideal effects such as viscous damping between buoy and power take-off, gearbox loss, generator loss, and power converter loss in the system are included in the circuit model with efficiencies from 60 - 80%. The maximum extracted power results under various wave conditions are dominated by these non-ideal effect.**

Keywords—**wave-to-wire model, PTO, tank test, power electronics, mechanical-motion-rectifier, equivalent circuit**

I. Introduction

Power electronics converter plays an important role in energy conversion and dynamic control in the WEC system, but it is seldom studied in the ocean energy field [1]–[5]. Due to the limit of the test equipment, most of the power electronics tests are realized with the motor – generator emulator in the lab [6]–[8], but usually the non-ideal dynamics of PTO or WEC are neglected compared to the wave-tank test or the ocean test. Wave-tank test provide a possibility to emulate the real wave condition before deploying the WEC system to the real ocean. The whole system is evaluated in the wave tank test from the buoy to the power converter, so the system characteristics and control verification be performed [9]–[11]. Wave tank test with PTO control is studied in [12] which is mainly focus on the harvesting the optimal power from the fluid-body dynamics through an ideal actuator (i.e. ideal PTO). However still very few studies on how the effects of the overall system including power electronics and PTO in the wave tank test.

This study shows a wave–to–wire test setup including the power electronics setup and wave-tank-test results. The circuit model [13] is derived from the PTO and WEC parameters. It is simulated and compared with the actual test results. The tank test is based on a 1:20 scale WEC system including buoy, PTO [14], and power converter based on the wave profile in Table 1. Passive damping control is applied due to the restriction on the mechanical-motion-rectifier (MMR) based PTO can only transfer the power from buoy to PTO [14].

In this paper the WEC is test under heave only 1DOF setup in the tank. Then a mechanical PTO along with the power electronics is built to charge a battery emulator. The frequency response and the design of digital controller of power converter are discussed in the following section. The wave-to-wire system including buoy, PTO, and power electronics is simplified to an equation based model with frictions. A linear circuit model is built accordingly to analyzed the optimal impedance in a system perspective. The analytical results and tested results are compared. The detailed W2W circuit model is introduced based on the experimental setups. The tank test results including the output power P_o on the battery, and the input power to the PTO P_{pto} are shown with different passive loadings and wave conditions. From the simulated result, the W2W circuit model approximates the force, maximum impedances for optimal output power from the tank test.

II. Setup of Wave-to-wire Tank Test

The wave tank test of a 1:20 scale WEC system is deployed in the wave tank for system identification and power converter testing.

Chien-An Chen is with the Center for Power Electronics Systems and the Bradley department of Electrical and Computer Engineering, Virginia Tech, Blacksburg, VA, 24061 U.S.A(e-mail: canchen@vt.edu).

Xiaofan Li, Dillon Martin, and Lei Zuo is with the Center for Energy Harvesting and Materials Systems and Mechanical Engineering, Virginia Tech, Blacksburg, VA, 24061 U.S.A. (e-mail: lixf@vt.edu; dilmart@vt.edu; leizuo@vt.edu).

TABLE I
TEST PROFILE OF 1:20 SCALE WEC

Wave ID	1/20th Scale Waves		Equivalent Full Scale Waves	
	Period (s)	Height (m)	Period(s)	Height (m)
M1	2.68	0.141	12.00	2.81
M2	3.13	0.191	14.00	3.83
M3	3.35	0.220	15.00	4.39
P1	3.47	0.260	15.50	5.20

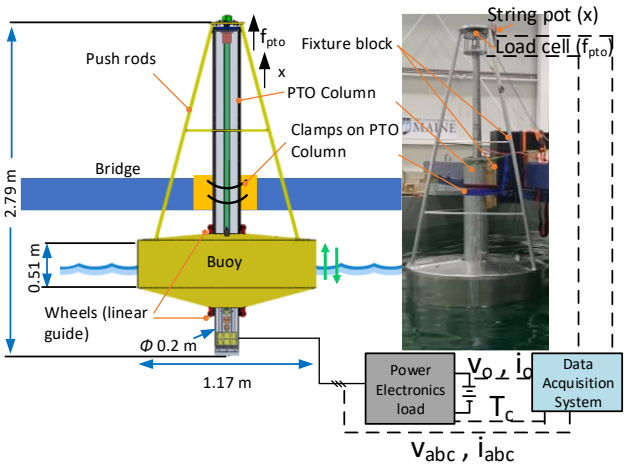

Fig. 1. Dimension and actual deployment of 1DOF 1:20 scale WEC in the wave tank with its relative position in Fig. 2. The connections of DAQ and power converter connection to the WEC are placed offshore.

A. *Setup of the buoy and PTO in the wave tank*

The buoy is test with 1DOF setup as shown in Fig. 1. The floating buoy has 1.17-meter diameter and the PTO column is clamped to the bridge. Thus the linear motion on the buoy transfers to the PTO column through the push rod, and the top and bottom wheels ensure the PTO column is driven in vertical directions. The PTO linear motions are transferred to rotary through ball- screw inside the PTO column. After that, the mechanical motion rectifier (MMR) gearbox converts the bidirectional motion to unidirectional rotation, and the generator is driven in one direction from the gearbox. The three phase output cables of the generator are sent offshore to the power electronics. The DAQ recorded the data during each run including the linear displacement of the PTO d_{pto} from which its linear velocity v_{pto} is derived through differentiation; the force to the PTO f_{pto} is measured through load cell; the output voltage and current are measured with shunt resistors; the case temperature of the IGBT module in the power converter is measured through thermal coupler; input voltages and currents to the power converter are measured separately through the oscilloscope. The sampling frequency of DAQ is 100 Hz, and the oscilloscope is set at 50 kHz for the power converter 15-kHz switching frequency.

The relative position of the deployed buoy in the water tank is shown in Fig. 2 which is place 11 meter from the wavemaker. The tank is 30-meter long, 9-meter wide, 4.5-meter deep, and with a 16-paddles flap-type wave maker and a beach at the end of the tank to cancel the wave reflections. The fixture block is built by steel structural I-beam and a wood block as an extension of thickness to fix the PTO column to the bridge. With its PTO column tied on the bridge in Fig. 1, the buoy was driven in heave only motion, and it is assumed that bridge and fixture block are fixed as one body.

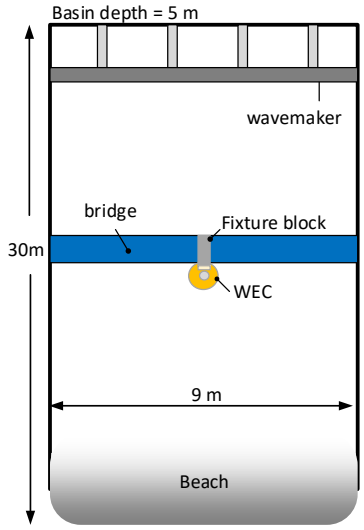

Fig. 2. Wave tank layout and dimensions at the University of Maine's Alfond W2 Ocean Engineering facility.

The WEC was tested under 3 regular wave conditions and 1 irregular wave condition as in Table I which are the 1:20 scaled down test conditions according the DOE Wave Energy Prize's [15] conditions. The monochromatic (regular) wave condition is tested for four minutes to ensure the buoy reach steady state, and the polychromatic (irregular) wave condition for 30 minutes. The irregular wave spectrum is created from Bretschneider spectrum [12].

B. *Setup of the power electronics*

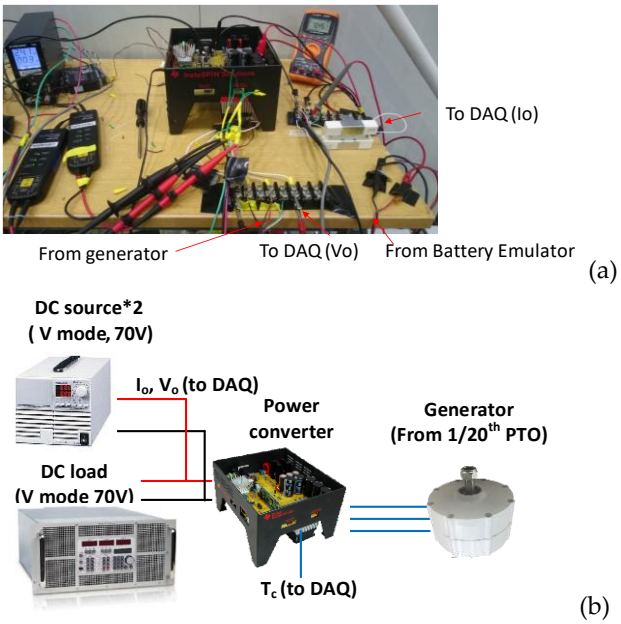

Fig. 3. Setup of power electronics. a) input and output power connections, and DAQ sensors connections, b) schematics from the generator in PTO - power converter – battery emulator, built by DC load and DC source with 70 V of constant voltage mode.

The 3-phase, 2-level power converter modified from a Texas Instrument high voltage development kit [16] as a generator rectifier in Fig. 3. The power converter is rated to 1000 W power, with connection to the 500 W permanent magnet synchronous generator (PMSG) inside PTO and output to the battery emulator as in Fig. 3(b). The battery emulator consists of a DC electronics load and a DC source, through the setup of DC load in constant voltage mode (CV) and DC source with constant voltage output at 70 V. The power flows from generator to the DC load through controlling the power converter with constant impedance mode to match the impedance with buoy and PTO, and the output current of the converter was measured through a 50 W/ 0.5 Ω shunt resistor connected in series with the DC load. The DC source is used to compensate the reactive power for field-oriented-control to ensure the maximum power is harvested with the minimum output current from the generator [17].

C. Controller design for the power converter

To design the controller for the power converter, an average circuit model in Fig. 4 is derived through the conventional three phase converter with battery and generator setup in d-q frame expression. The small signal model from the PWM duty to current is written in (1) by assuming $i_d = 0$, and v_{dc} is constant with battery load. Its frequency response is plotted in Fig. 5 with originally 5 kHz of bandwidth. To compensate the DC gain and phase margin in the closed loop, a compensator with transfer function $G_c(s)$ is deployed to the control loop. The loop gain $G_L(s)$ from (2) has an infinite DC gain 2 kHz of bandwidth, and 100 degree of phase margin in the frequency response in Fig. 5.

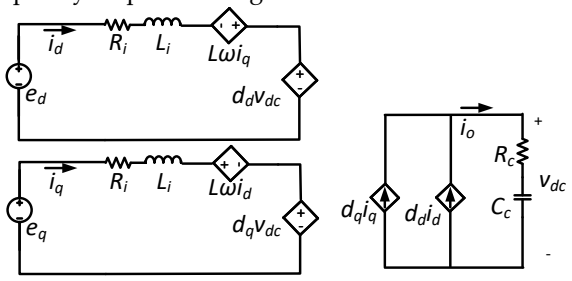

Fig. 4. Average model of the power converter with generator input and battery output according the switching-model circuit and the electrical part of the generator in Fig. 9.

$$G(s) = \frac{i_q(s)}{\mathrm{d}_q(s)} = \frac{-V_{dc}}{(R_i + sL_i)} = \frac{-\frac{V_{dc}}{R_i}}{1+\frac{L_i}{R_i}s} \quad (1)$$

$$G_L(s) = G(s)G_c(s) \quad (2)$$

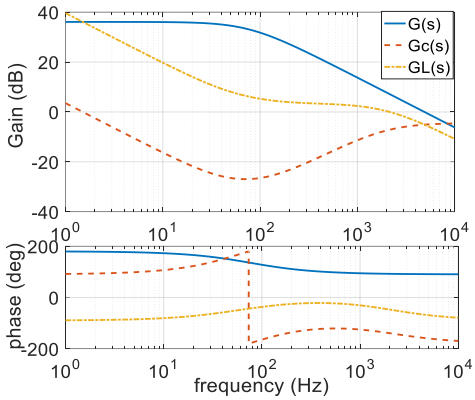

Fig. 5. Frequency response of the power converter from the small signal model $G(s)$ in (1), the compensator $G_c(s)$, and the loop gain with the compensator $G_L(s) = G(s)\,G_c(s)$ in (2).

III. ANALYSIS OF SIMULATION AND TANK TEST RESULT

Tank test results are shown in this section with comparison of calculation results and simulation results

A. Equivalent circuit and suboptimal passive loading for calculations

The circuit model is used to derived the equation for suboptimal power estimation with passive loading, and its calculation results are compared with the tank test results.

From Fig. 9, the simplified equivalent circuit model in Fig. 6 is developed which includes the non-ideal effects in the PTO, the circuit model for fluid – body dynamics, and the impedance to the power converter is controlled as Z_{inp} equals to the sum of R_{ip} and R_e in the figure. The diodes and inductors are omitted in the Fig. 9 due to low driving frequency, and transformers are eliminated by converting all the parameters the buoy side of the circuit. The output power of the power converter P_o is written in (3) as a result from the i_e (the excitation force to the buoy) and viscous damping in between where the Z_x is the impedances of buoy and PTO; s equals to jω, ω is the wave frequency in rad/s; R_{ip}, Z_{inp} is the equivalent generator internal resistance and the equivalent controlled impedance of the power converter seen from the buoy; C_{Jm} is the equivalent inertia from the generator; k_b is the linear – rotary ratio of the ball-screw; k_g is the gear ratio of gearbox; the generator ratio $k_{ge} = 3p\,K_e\,K_t/32$; p, K_e, K_t are listed in the Table II.

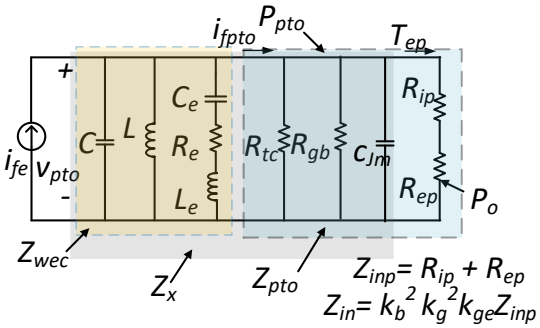

Fig. 6. Simplified circuit model of the WEC from Fig. 9 for the suboptimal passive loading calculation.

$$P_o = i_{fe}{}^2[\frac{Z_x}{Z_x + (R_{ip} + R_{ep})}]^2 R_{ep} \quad (3)$$

$$Z_x = \frac{1}{s(C + C_{Jm}) + \frac{1}{R_{gb}} + \frac{1}{R_{tc}} + \frac{1}{sL} + \frac{1}{R_e + sL_e + \frac{1}{sC_e}}} \quad (4)$$

$$Z_{inp} = (R_{ip} + R_{ep}) \quad (5)$$

$$Z_{in} = k_b{}^2 k_g{}^2 k_{ge} Z_{inp} \quad (6)$$

$$\frac{dP_o}{dZ_{inp}} = \frac{d[\frac{Z_x}{Z_x + (R_{ip} + R_{ep})}]^2 R_{ep}}{dZ_{inp}} = 0 \quad (7)$$

As a result, the maximum output power is derived from (7) with the optimal passive loading Z_{in} is plotted on Fig. 8 in comparison with the tank test results. The calculated P_o are more than the tested result due to the lack of the model on other practical damping during the test such as the damping/friction from the wheels, or the drag force on the buoy. While the calculation results in Fig. 8 (a) still shows a closed optimal loading $Z_{in(s)}$ (around 3 – 4 Ω) to the optimal loading in the tank test (around 5 Ω).

The input power to the PTO - P_{pto} is written in (8) with $Z_{wec}(s)$ equals to v_{pto}(s) / i_{fe}(s) as the impedance of buoy which is an analogy of ẋ(s) / f_e(s), where the v_{pto} and f_e are the velocity and excitation force. Similar analogies from WEC dynamics to circuit model is found in [18] and [19]. The buoy impedance Z_{wec}(s) is defined under the assumption of open circuit on PTO terminal i.e. $i_{fpto} = 0$. The values in Fig. 6 of the $Z_{wec}(s)$ are derived from WAMIT model and network synthesis process. The impedance $Z_{wec}(s)$ in Fig. 7 shows that the resonant period of the buoy is around 1.5 second. In the tank test condition M2, 3.13 second of period, the magnitude of the impedance is -71.6 dB which is around 3833 Ns/m of damping at the given frequency. From (10) and (11), the optimal power occurs when the PTO damping Z_{pto} equals to the Z_{wec}, where Z_{pto} consists not only the impedance from the power converter, and the mechanical damping/frictions of the PTO transmission are considered.

The results of P_{pto} from analytical model (8) and tank test are shown in Fig. 8(b) where two curves have similar optimal passive loading Z_{in} (around 2 – 3 Ω).

$$P_{pto}(s) = i_{fe}(s)^2[\frac{Z_{wec}(s)}{Z_{wec}(s) + Z_{pto}(s)}]^2 Z_{pto}(s) \quad (8)$$

$$Z_{wec}(s) = \frac{v_{pto}(s)}{i_{fe}(s)} = \frac{1}{sC + \frac{1}{sL} + \frac{1}{R_e + sL_e + \frac{1}{sC_e}}} \quad (9)$$

assuming $i_{fpto} = 0$

$$Z_{pto}(s) = \frac{v_{pto}(s)}{i_{fpto}(s)} = \frac{1}{sC_{Jm} + \frac{1}{R_{gb}} + \frac{1}{R_{tc}} + \frac{1}{Z_{inp}}} \quad (10)$$

$$\frac{dP_{pto}}{dZ_{inp}} = \frac{d[\frac{Z_{wec}}{Z_{wec} + Z_{pto}}]^2 Z_{pto}}{dZ_{inp}} = 0 \quad (11)$$

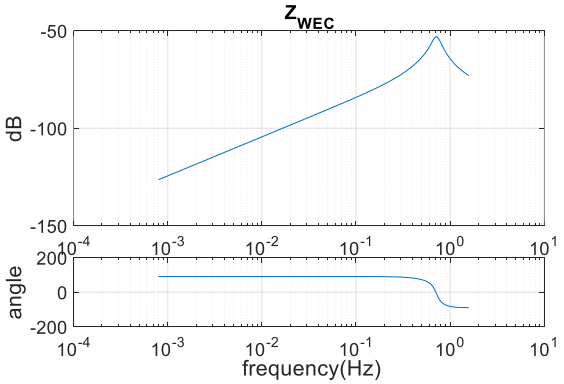

Fig. 7. Frequency response of the WEC buoy dynamics from the equivalent current i_{fe}(s) of wave excitation force to the equivalent voltage v_{pto}(s) of buoy velocity where Z_{wec}(s) = v_{pto}(s)/ i_{fe}(s) as shown in Fig. 6 is equivalent to the impedance from the circuit model.

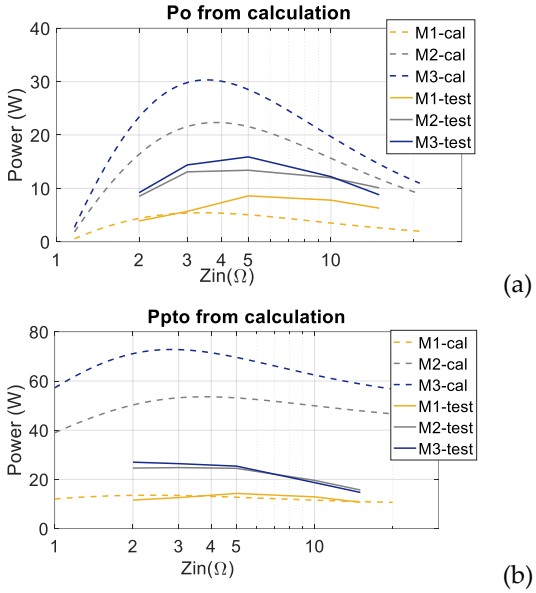

Fig. 8. Electrical output power and PTO input power from the calculations (dotted lines) through (3) and (8), and tank test results (solid lines).

Differences are shown in Fig. 8 between the tank-test results and the analytical results from (3) and (8) especially when with higher driving frequency, e.g. M2 and M3. The differences are mainly from the non-linearity of the MMR is more obvious in higher frequency due the higher disengagement ratio [14]. The analytical results are still a useful tool to estimate the optimal impedance Z_{in} (damping) for a maximum output power P_o. The circuit model considering MMR dynamics shows a better prediction of trend on P_o and P_{pto}.

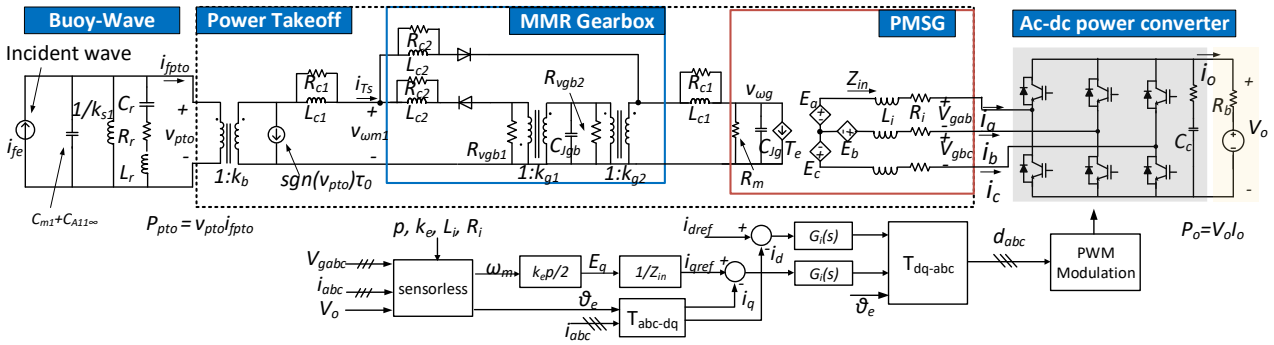

Fig. 9. Wave- to –wire equivalent model for circuit-based simulations from fluid to body – PTO – generator – power converter – battery. The control algorithm of the power converter includes sensorless control, field oriented control, and space vector pulse width modulation (PWM) as passive loading control for the input impedance Z_{in} sweeping under various wave conditions. The parameters values are shown in the table from the appendix. The simulation results are shown in Fig. 10 – 12 using v_{pto} from tank test as input.

B. *Tank test results and simulation model*

The tank-test results are compared with the simulated results in this section. The simulation circuit model is derived in [12] from the bench test of the PTO in Fig. 9 which is an analogy of buoy dynamics and the MMR based PTO. It models the mechanical components such as mechanical coupling, one-way bearing, ball screw, and gearbox to equivalent circuit network. The model predicts the efficiency and the input force of the PTO by considering the non-ideal effects from the mechanical transmission including fictions, damping, and compliances in the mechanical components. Along with the power electronics circuits, a simulation model is built for the electrical based simulation, and the controller for the power converter is designed in the model. The velocity measured from the tank test is applied as an input to the model. The output power P_o of the converter and the input power P_{pto} to the PTO are compared between the simulation and tank test results in Fig. 10.

The simulation results show high consistency with the test results on the input power P_{pto} to the PTO in Fig. 10(a). This simulated P_{pto} shows that the maximum input power to PTO occurs when Z_{in} is around 2 Ω

While the results on output power shows around 5 – 10 W of errors between testing and simulation which might due to the high electromagnetic noise contaminate the measured current signal to the DAQ. Therefore, the test data is higher than the simulated data in Fig. 10 (b). Even through the mismatch on the simulated data of output power, it predicts the optimal power damping on various wave conditions, where all the maximum power point occurs when Z_{in} equals to 5 Ω.

The difference between the maximum P_{pto} and the maximum P_o shows that the optimal impedances Z_{in} are different in when using different power as criteria. The optimal power harvested by the battery P_o is decided not only by the overall damping from the PTO, but the non-ideal effects in the PTO transmission.

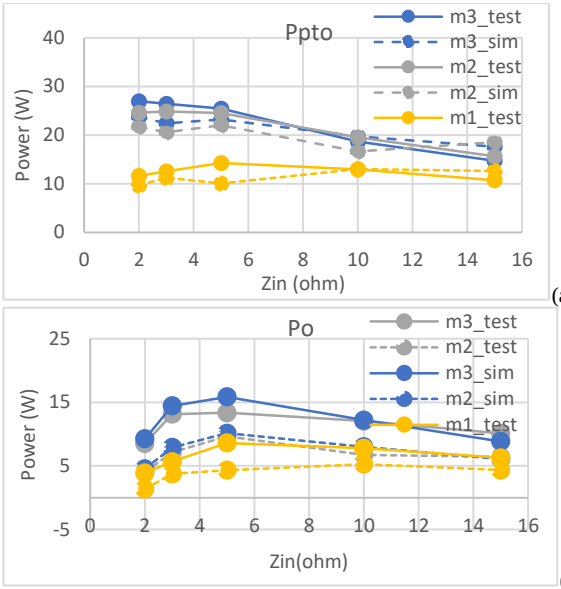

Fig. 10. The tank test results and simulation results of the circuit model in Fig. 9 using the measured v_{pto} from tank test as input, a) The input power of PTO P_{in}, and b) the output power to the battery P_{oe}.

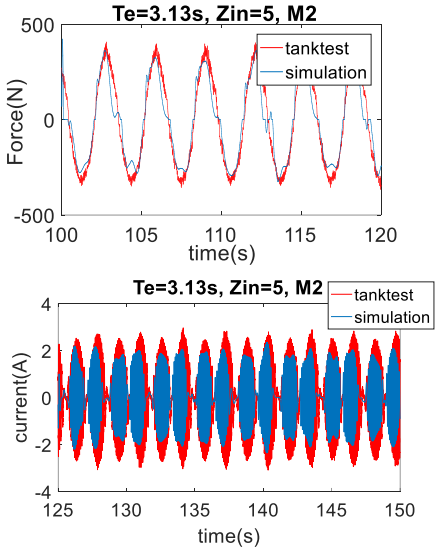

Fig. 11. The time domain results from tank test and simulation with Fig. 9 circuit model showing the PTO force f_{pto} (i_{fpto})and output current of the generator i_a under M2 condition (Table I) with input impedance Z_{in} equals to 5 ohm.

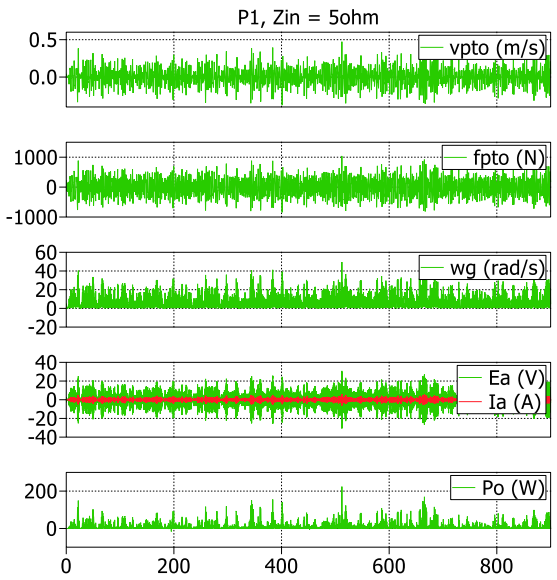

Fig. 12. Simulation results with irregular wave condition P1 from Tabel I, and input impedance Z_{in} = 5 Ω (passive control).

The prediction of the circuit model in time domain is shown in Fig. 11 that the PTO input force and output current from the generator are approximated to the results from the tank test. Finally, the W2W model is used to estimate the irregular wave dynamics from the given PTO velocity to PTO force, all the way down to the output power of the power converter.

IV. CONCLUSION

A wave-to-wire test is performed in the wave tank. The power electronics setup is introduced with its controller design. A circuit simulation model and equation model is built from the parameters of 1:20 scale WEC and PTO. These model includes the non-ideal effects in PTO showing its predictive capability on comparison between simulation/calculation and test results.

APPENDIX

TABLE II
SETUP PARAMETERS OF THE WEC

PMSG	NE 600W	
IGBT module	ps21765	
Battery emulator Voltage	E_b	70 V
Switching frequency	f_{sw}	15 kHz
Internal resistor of PMSG	Ri	1.1 Ω
Internal inductor of PMSG	Li	2.3 mH
Voltage constant of PMSG	K_e	0.104
Torque constant of PMSG	K_t	0.104
Pole pairs of PMSG	p	6
Inertia of generator	J_g	0.013 kgm^2
Dc bus capacitance	C_c	1950 μF
Battery emulator resistance	R_b	0.2 Ω
gear ratio of gearbox	k_g	1
Linear-rotary ratio of ball screw	k_b	104
Mass of buoy	m_1	266
Compensator for current loop controller: $G_c(s)$ =	$\frac{s^2 + 942s + 2e5}{s^2 + 1.25e4s}$	

ACKNOWLEDGEMENT

The authors gratefully acknowledge the support and funding from the U.S. Department of Energy (DOE). Authors would like to thank Mr. Mathew Cameron, Mr. Matthew Fowler, Dr. Krish Thiagarajan, and Dr. Xiuxing Yin for their support during the wave tank testing.

REFERENCES

[1] H. Mendonca and S. Martinez, "A resistance emulation approach to optimize the wave energy harvesting for a direct drive point absorber," *IEEE Trans. Sustain. Energy*, vol. 7, no. 1, pp. 3–11, 2016.

[2] C. Boström, E. Lejerskog, M. Stålberg, K. Thorburn, and M. Leijon, "Experimental results of rectification and filtration from an offshore wave energy system," *Renew. Energy*, vol. 34, no. 5, pp. 1381–1387, 2009.

[3] M. Leijon, O. Danielsson, M. Eriksson, K. Thorburn, H. Bernhoff, J. Isberg, J. Sundberg, I. Ivanova, E. Sjöstedt, O. Ågren, K. E. Karlsson, and A. Wolfbrandt, "An electrical approach to wave energy conversion," *Renew. Energy*, vol. 31, no. 9, pp. 1309–1319, 2006.

[4] J. Sjolte, C. M. Sandvik, E. Tedeschi, and M. Molinas, "Exploring the potential for increased production from the wave energy converter lifesaver by reactive control," *Energies*, vol. 6, no. 8, pp. 3706–3733, 2013.

[5] E. Tedeschi, M. Carraro, M. Molinas, and P. Mattavelli, "Effect of control strategies and power take-off efficiency on the power capture from sea waves," *IEEE Trans. Energy Convers.*, vol. 26, no. 4, pp. 1088–1098, 2011.

[6] S. Hazra, P. Kamat, and S. Bhattacharya, "A partially-rated active filter enabled power architecture to generate oscillating power from wave energy converter," *ECCE 2016 - IEEE Energy Convers. Congr. Expo. Proc.*, 2016.

[7] Z. Nie, X. Xiao, R. McMahon, P. Clifton, Y. Wu, and S. Shao, "Emulation and control methods for direct drive linear wave energy converters," *IEEE Trans. Ind. Informatics*, vol. 9, no. 2, pp. 790–798, 2013.

[8] J. K. H. Shek, D. E. Macpherson, and M. A. Mueller, "Experimental verification of linear generator control for direct drive wave energy conversion," *IET Renew. Power Gener.*, vol. 4, no. 5, p. 395, 2010.

[9] B. Bosma, T. Lewis, T. Brekken, and A. von Jouanne, "Wave Tank Testing and Model Validation of an Autonomous Wave Energy Converter," *Energies* , vol. 8, no. 8. 2015.

[10] J. H. Todalshaug, G. S. Ásgeirsson, E. Hjálmarsson, J. Maillet, P. Möller, P. Pires, M. Guérinel, and M. Lopes, "Tank testing of an inherently phase-controlled wave energy converter," *Int. J. Mar. Energy*, vol. 15, pp. 68–84, 2016.

[11] D. Martin, X. Li, C.-A. Chen, X. Yin, R. Parker, K. D. T. Ngo, K. P. Thiagarajan, and L. Zuo, "Wave Tank Experimentation of a Two-Body Point Absorber," in *Marine Energy Technology Symposium (METS)*, 2018.

[12] M. J. Tucker and E. G. Pitt, *Waves in Ocean Engineering*. UK: Elsevier Science, 2001.

[13] C.-A. Chen, X. Li, Z. Lei, and K. Ngo, "Equivalent Circuit for Mechanical-Motion Rectifier Based Power Take-off in Wave Energy Harvesting," in *AWTEC*, 2018.

[14] X. Li, C. Liang, J. Boontanom, D. Martin, K. Ngo, R. Parker, and L. Zuo, "Design , fabrication and testing of wave energy converters using different power take-off with

mechanical motion rectifier," in *European Wave and Tidal Energy Conference (EWTEC)*, 2017, pp. 1–7.

[15] Wave Energy Prize, "Wave Energy Prize Rules," in *U.S. Department of Energy*, 2016.

[16] "http://www.ti.com/tool/TMDSHVMTRINSPIN." .

[17] C. Capitan, "Torque Control in Field Weakening Mode," no. June, p. 84, 2009.

[18] J. Sjolte, I. Bjerke, A. Crozier, G. Tjensvoll, and M. Molinas, "All-electric wave energy Power Take Off system with improved power quality at the grid connection point," in *PES T&D 2012*, 2012, pp. 1–7.

[19] L. Hai, O. Svensson, J. Isberg, and M. Leijon, "Modelling a point absorbing wave energy converter by the equivalent electric circuit theory: A feasibility study," *J. Appl. Phys.*, vol. 117, no. 16, 2015.